Journal of Alloys and Compounds 794 (2019) 615–624

Contents lists available at ScienceDirect

Journal of Alloys and Compounds

journal homepage: http://www.elsevier.com/locate/jalcom

Microstructure and Vickers hardness of mechanically alloyed and spark plasma sintered Ti-2Zn-22Si-11B and Ti-6Zn-22Si-11B alloys

Nelson Damásio Ferreira [a], Ricardo Mendes Leal Neto [b], Marcello Filgueira [c], Lucas Moreira Ferreira [d], Manuel Fellipe Rodrigues Pais Alves [d], Erika Coaglia Trindade Ramos [a], Carlos Angelo Nunes [d], Claudinei dos Santos [d], Alfeu Saraiva Ramos [a, *]

[a] Universidade Federal de Alfenas, Instituto de Ciência e Tecnologia, Rod. José Aurélio Vilela, 11999, Poços de Caldas, MG, 37715-400, Brazil
[b] Instituto de Pesquisas Energéticas e Nucleares, Centro de Ciência e Tecnologia de Materiais, Av. Prof. Lineu Prestes, 2242, São Paulo, SP, 05508-000, Brazil
[c] Universidade Estadual do Norte Fluminense, Centro de Ciência e Tecnologia, Av. Alberto Lamego, 200, Campos dos Goytacazes, RJ, 28013-602, Brazil
[d] Universidade de São Paulo, Departamento de Engenharia de Materiais, Polo Urbo-Industrial, Gleba AI-6, 12600-970, Lorena, SP, Brazil

ARTICLE INFO

Article history:
Received 2 September 2018
Received in revised form
12 April 2019
Accepted 16 April 2019
Available online 19 April 2019

Keywords:
Ti_6Si_2B
Zinc
Mechanical alloying
Spark plasma sintering

ABSTRACT

This work reports on effect of zinc and milling time on microstructure and Vickers hardness of mechanically alloyed and spark plasma sintered (66,7-x)Ti-xZn-22,2Si-11,1B alloys (at.-%, with x = 2 and 6 at.-%). Ball milling at different times (20, 60, 180 and 300 min) was performed under argon atmosphere in a planetary ball mill from these elemental powder mixtures. Cylinder bodies with 10 mm diameter were consolidated by spark plasma sintering (1100 °C, 12 min, 20 MPa) under argon atmosphere. As-milled powders and sintered Ti-Zn-Si-B samples were evaluated by X-ray diffraction, scanning electron microscopy, energy dispersive spectrometry, laser diffraction particle size analysis, and Vickers hardness tests. It was noted a similar behavior during ball milling of Ti-Zn-Si-B powder mixtures. Only the α-Ti and Si peaks were indexed in XRD patterns of Ti-Zn-Si-B powders milled for 300 min. Rietveld refining indicated that the amount of amorphous structures has increased during milling up to 300 min, which was more pronounced for the Ti-6Zn-22Si-11B powders. The particle sizes of the Ti-2Zn-22Si-11B and Ti-6Zn-22Si-11B powder mixtures increased during milling from 94 (20 min) to 156 (300 min) μm and from 101 (20 min) to 136 (300 min) μm, respectively. Coherently, the average specific surface area of powder particles was continuously reduced during milling. Despite the adopted parameters, the SPS process produced dense Ti-xZn-22Si-11B (x = 2 and 6 at.-%) alloys with 98% from their theoretical specific mass. Regardless of milling time, the Ti_6Si_2B formation was inhibited in microstructure of the spark plasma sintered Ti-6Zn-22Si-11B alloy previously milled for longer times. EDS analysis indicated that the Ti_6Si_2B phase dissolved close to 1.8 at.-% Zn. Beside the TiB and Ti_5Si_3, the Ti_2Zn and Ti_3Zn (not explored) phases were also found in microstructure of sintered Ti-Zn-Si-B alloys. The Ti-2Zn-22Si-11B alloy presented average Vickers hardness values higher than 1050 HV whereas the Ti-6Zn-22Si-11B alloy varied between 970 and 1036 HV, which could be associated with the Ti_6Si_2B formation.

1. Introduction

Titanium alloys with addition of Nb, Ta, Zr, Mo and/or others alloying are alloy designs based on substitutional solid solutions [1–6], which present limited properties for use in medical articular implants under loading. In the Ti-Si-B system, the two-phase (Ti + Ti_6Si_2B) or three-phase (Ti-Ti_6Si_2B + TiB) alloys are produced by conventional techniques such as arc melting and mechanical alloying [7,8]. Previous works have reported that the Ti-10Si-5B implants presented superior bone integration than

* Corresponding author.
E-mail addresses: nelsondamasio@gmail.com (N.D. Ferreira), lealneto@ipen.br (R.M. Leal Neto), marcello@uenf.br (M. Filgueira), lucasmofe@gmail.com (L.M. Ferreira), manuelfelipealves@gmail.com (M.F. Rodrigues Pais Alves), erika.ramos@unufal-mg.edu.br (E.C. Trindade Ramos), cnunes@demar.eel.usp.br (C.A. Nunes), claudineisvr@gmail.com (C. Santos), alfeu.ramos@unifal-mg.edu.br (A.S. Ramos).

https://doi.org/10.1016/j.jallcom.2019.04.172
0925-8388/

conventional titanium implants beside its lower friction coefficient and higher wear resistance [9,10].

In order to develop new multicomponent Ti_6Si_2B-based titanium alloys different studies involving the alloying addition have been reported [11–13]. In Ti-xMe-22Si-11B (Me = Zr, Nb, Mo, Ta) alloys, the Ti_6Si_2B phase was formed in Ti-xZr-22Si-11B compositions with x up to 7 at.-% Zr. In the quaternary alloys with addition of Nb, Ta or Mo, the undesirable Ti_5Si_3 phase is preferentially formed during sintering for compositions with alloying (Me − Nb, Ta, Mo) higher than 2 at.-%.

Zinc is essential for bone healing and its increased amounts are found at the sites of bone repair, and the low levels in the body have been closely linked with osteoporosis [14]. According to the phase diagram of the Ti-Zn system [15], the titanium dissolves close to 6 at.-% Zn and the following intermediate phases are reported: Ti_2Zn, TiZn, $TiZn_2$, $TiZn_3$, $TiZn_5$, $TiZn_{10}$, and $TiZn_{16}$. Others studies have indicated that zinc is immiscible for both the boron [16] and silicon [17]. The present work aims to investigate on effect of zinc addition on composition and milling time on microstructure and Vickers hardness of mechanically alloyed and spark plasma sintered (67-x)Ti-xZn-22Si-11B (x = 2 and 6 at.%) alloys.

2. Materials and methods

The following raw materials were used in this work for preparing the Ti-2Zn-22Si-11B and Ti-6Zn-22Si-11B (at.-%) by high-energy ball milling and subsequent spark plasma sintering: Ti (99.9 wt.-%, spherical, <150 mesh), Zn (min 99.8 wt.-%), Si (99.999 wt.-%, irregular, <150 mesh), and B (99.5 wt.-%, angular, <150 mesh).

The Ti-Zn-Si-B powder mixtures were processed under argon atmosphere in a planetary Fritsch P-5 ball mill using tungsten carbide vial (225 mL) and balls (10 mm diameter), a ball-to-powder ratio of 10:1, and rotatory speed of 300 rpm. Samples were milled at different times: 20, 60, 180 and 300 min.

In the sequence, the as-milled Ti-Zn-Si-B powders were spark plasma sintered (SPS) under vacuum (10^{-2} mbar) in a Dr. Sinter – fdc SPS division model sps-211lx sintering machine using heating (~65 °C/min) up to 1100 °C for 12 min, pressure of 20 MPa and a graphite matrix.

To remove the C-rich surface layer of spark plasma sintered Ti-Zn-Si-B samples their metallographic preparation was made with SiC papers until #4000 for further polishing with 0.3 μm Al_2O_3 suspension.

The as-milled Ti-Zn-Si-B powders and SPS samples were characterized by X-Ray diffraction (XRD), scanning electron microscopy (SEM), energy dispersive spectrometry (EDS), laser diffraction particle size analysis, and Vickers hardness.

XRD experiments at room temperature were performed in a Panalytical Empyrean equipment using Cu-Kα radiation (Kα1 = 1,540598 Å and Kα2 = 1,544426 Å), voltage of 40 kV, current of 30 mA, diffraction angle (2θ) varying between 20 and 80°, angular pass of 0.02° and counting time per pass of 80s. The relative amount of phases and their lattice parameters and interplanar distance were determined in X-ray experiments was determined by Rietveld refinement [18], on the *X'pert Hightscore* software from Phillips, adopting the peaks like pseudo-Voigt type shape. Furthermore, the percentage of crystalline phases in a multiphase

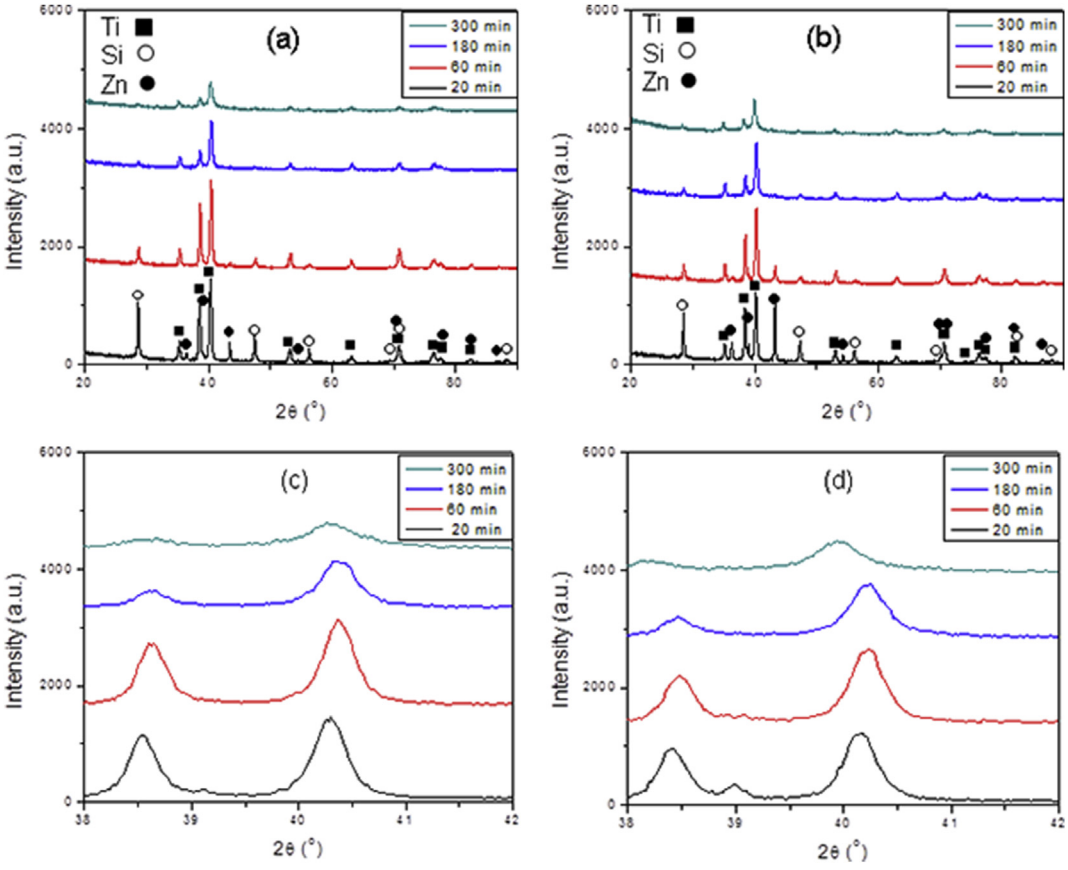

Fig. 1. XRD patterns of (a) Ti-2Zn-22Si-11B and (b) Ti-6Zn-22Si-11B powders at different milling times. Details on their major α-Ti peaks are illustrated in (c) and (d), respectively.

Table 1
Effect of composition and milling time on the lattice parameters and unit cell volume of α-Ti, Si and Zn obtained by Rietveld refinement.

	Milling time (min)	Ti space group (194)	Si space group (227)	Zn space group (194)	Rp	Rwp	Re	χ^2
65Ti-2Zn-22Si-11B	20	a = 2,9512 Å c = 4,6868 Å V = 35.3539 Å^3	a = 5.43135 Å V = 160.2229 Å^3	a = 2.6654 Å c = 4.9622 Å V = 30.5198 Å^3	19.8	27.2	24.1	1.6
	60	a = 2.9521 Å c = 4.6834 Å V = 35.3494 Å^3	a = 5.4312 Å V = 160.2093 Å^3	a = 2.6626 Å c = 4.9716 Å V = 30.5253 Å^3	19.2	25.0	23.7	1.4
	180	a = 2.9510 Å c = 4.6833 Å V = 35.3221 Å^3	a = 5.42957 Å V = 160.0648 Å^3	*	35.9	46.7	32.5	2
	300	a = 2.9504 Å c = 4.6834 Å V = 35.3074 Å^3	a = 5.42894 Å V = 160.009 Å^3	*	31.6	42.1	31.8	1.7
62Ti-6Zn-22Si-11B	20	a = 2,9503 Å c = 4,6842 Å V = 35.3107 Å^3	a = 5.42627 Å V = 159.8133 Å^3	a = 2.6629 Å c = 4.9465 Å V = 30.3769 Å^3	33.4	43.5	22.2	3.2
	60	a = 2.9498 Å c = 4.683 Å V = 35.2942 Å^3	a = 5.42539 Å V = 159.6955 Å^3	a = 2.6658 Å c = 4.9471 Å V = 30.4474 Å^3	20.88	34.5	27.7	2.8
	180	a = 2.9501 Å c = 4.6821 Å V = 35.2901 Å^3	a = 5.42298 Å V = 159.4825 Å^3	a = 2.6653 Å c = 4.9621 Å V = 30.5198 Å^3	11.8	14.5	11.2	1.7
	300	a = 2.9491 Å c = 4.6786 Å V = 35.2443 Å^3	a = 5.42196 Å V = 159.3927 Å^3	*	32.6	42.7	30.5	1.9

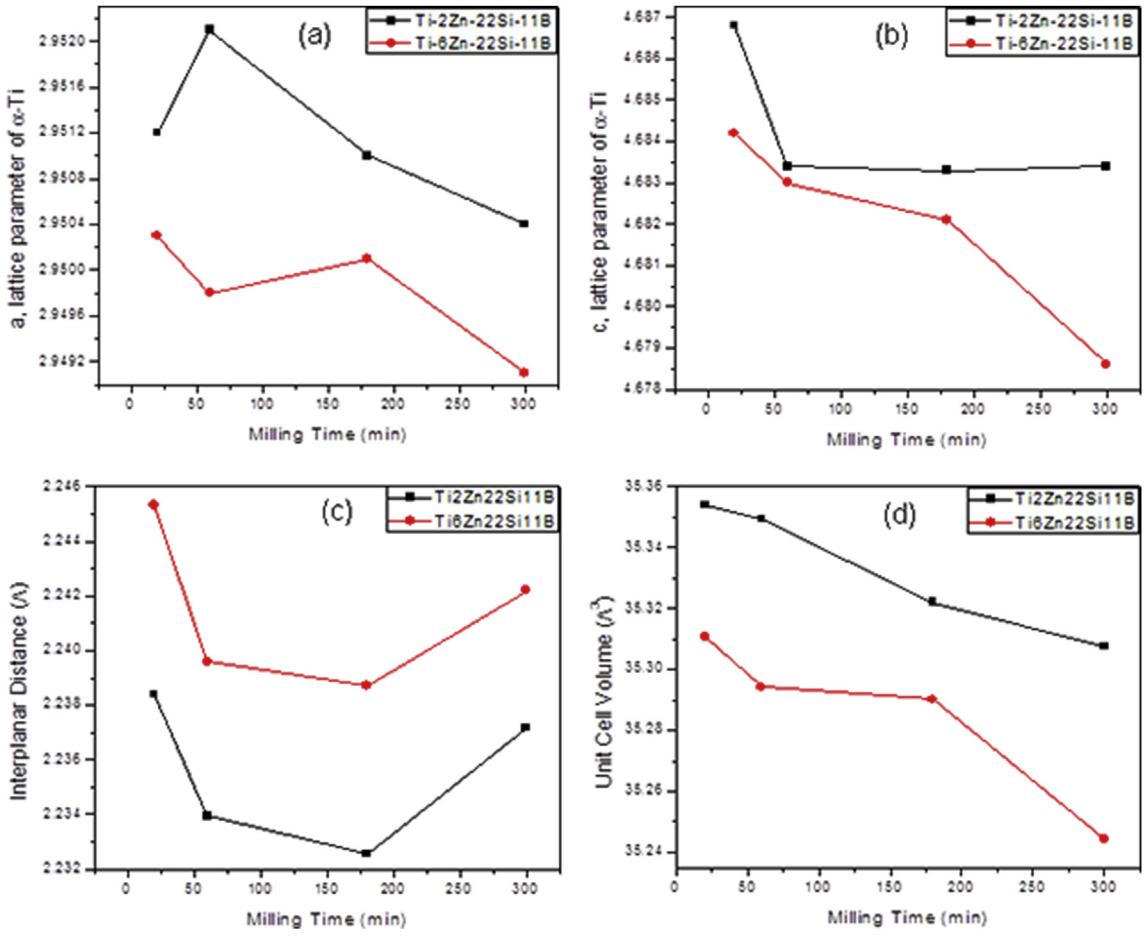

Fig. 2. Effect of composition and milling time on the (a, b) lattice parameters, (c) interplanar distance and (d) unit cell volume of α-Ti measured by Rietveld refinement.

material was calculated as described by Hill and Howard [19].

$$W_P = \frac{S_P.(Z.M.V)}{\sum_{i=1}^{n} S_i.(Z.M.V)}.100 \quad (1)$$

Where: Wp = percentage of "p" phase (by weight) in the mixture of "n" phases; S = Rietveld scale factor; Z = number of formulas per unit cell; M = mass of each formula; V = unit cell volume. After removing the contribution of the k-alpha 2 to the obtained data, the full widths at half maximum (FWHM) were calculated by the integral method. The crystallite sizes of α-Ti in Ti-Zn-Si-B samples were estimated by the Scherrer equation disregarding the instrumental broadening of diffraction peaks [20]. Some agreement indices are usually applied in the Rietveld refinement to quantitatively measure the quality of the refinement [21–23]. The R_{wp} (Weighted Profile R-Factor) indice is a correlation of the observed intensity for each phase, and the weighted fraction of each phase, with the calculated intensities. The R_{exp} (Expected R-Factor) indice is the ideal model for the collected data, the best possible R_{wp} the data could be achieved. So, the term called χ^2 (Good of Fitness) is the correlation between the R_{wp} and the R_{exp} and it describes how good the simulated diffractogram fit in the measured diffractogram, by the formula $\chi^2 = (R_{wp}/R_{exp})^2$.

SEM images and EDS microanalysis of as-milled and SPS Ti-Zn-Si-B samples were obtained in a Hitachi model TM3000 equipment using back-scattered electrons detector and the EDS measurements of phases presents in SPS samples were performed using inner patterns in terms of Ti, Zr and Si.

The particle size distribution of Ti-Zn-Si-B powder mixtures were measured by laser diffraction analysis in a Malvern model Mastersizer 2000 equipment using the Fraunhofer method and water as dispersant.

The Vickers hardness tests of spark plasma sintered Ti-Zn-Si-B alloys were conducted in a Vickers microhardness tester model TIME F100, in accordance with the ASTM C 1327-15 standard [24] using a load of 9.81 N. Ten indentations were made in each sample in order to evaluate its homogeneity: five indentations were made along the horizontal section and another five along the vertical section of the specimens.

3. Results

XRD patterns of Ti-2Zn-22Si-11B and Ti-6Zn-22Si-11B powder mixtures milled for different times are presented in Fig. 1a and. 1b, respectively. As expected, the Zn peaks were more intense in the Zn-richer powder mixture. Similar behavior was found during milling of Ti-Zn-Si-B powders, i.e., the Ti peaks were broadened and had their intensities reduced for longer milling times. After milling for 300 min, it can be noted that the peaks of zinc disappeared beside the Si traces only. No intermetallic peak was identified in powders milled for 300 min. In addition, the α-Ti peaks were moved toward the higher diffraction angles in powders milled for 60 and 180 min suggesting that elemental dissolution into the Ti lattice was achieved (see Fig. 1c and d). Ti, Zn, Si and B exhibit atomic (and covalent) radium of 140 (136), 134 (122), 111 (111) and 87 (62), respectively. Table 1 shows the lattice parameters and unit cell volume of α-Ti, Si and Zn obtained by Rietveld refinement whereas Fig. 2 is illustrating the effect of composition and milling time on the lattice parameters, interplanar distance and unit cell volume of α-Ti. It was noted that the interplanar distance of α-Ti was continuously reduced up to 180 min and furtherly increased after milling for 300 min (Fig. 2c). Coherently, its lattice parameters and unit cell volume have reduced during ball milling indicating that supersaturated solid solutions were formed in severely deformed structures, which was more pronounced for the Ti-6Zn-22Si-11B powders (Fig. 2a, b and 2d). Consequently, the amount of amorphous phase was increased in these Zn-richer powders (Fig. 3a). The crystallite sizes of Ti were reduced from 250 (240) nm to 130 (110) nm in Ti-6Zn-22Si-11B (Ti-2Zn-22Si-11B) powders milled for 300 min as are illustrated in Fig. 3b.

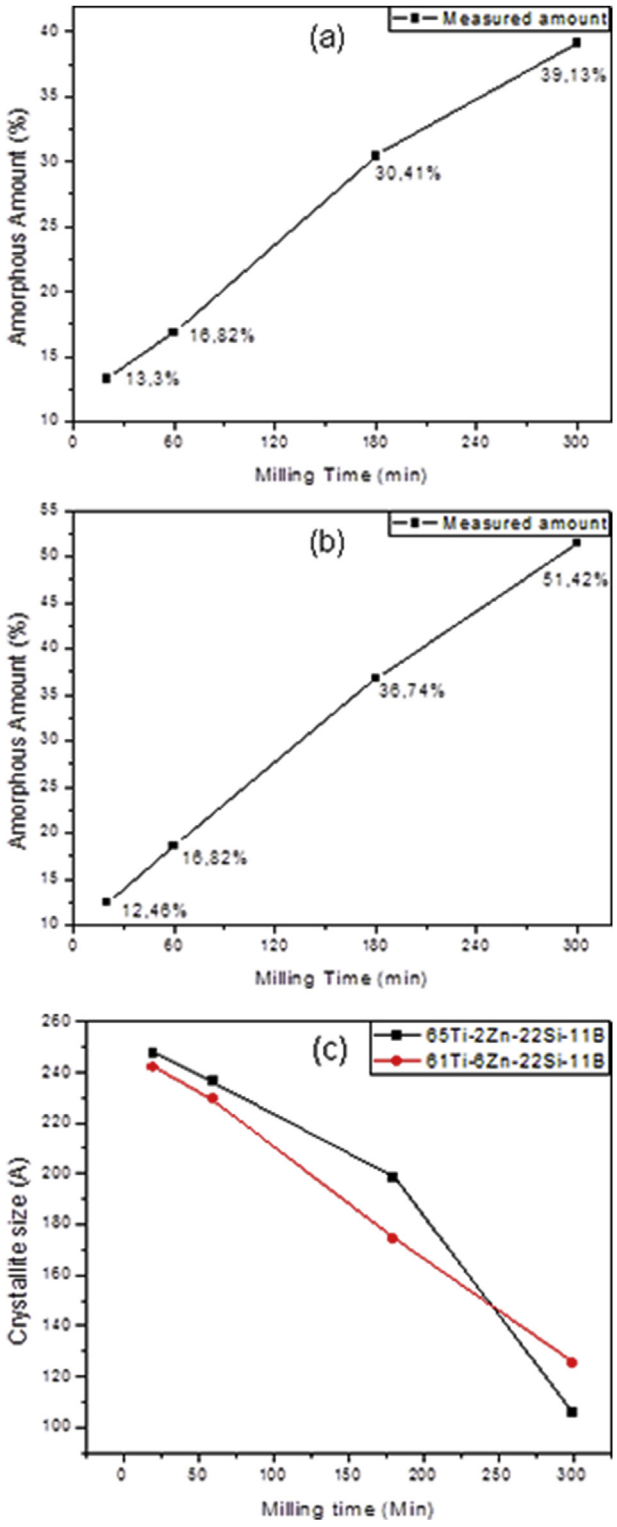

Fig. 3. Effect of composition and milling time on (a, b) amount of amorphous phase content in Ti-2Zn-22Si-11B and (b) Ti-6Zn-22Si-11B powders, and (c) the crystallite sizes of α-Ti after different milling times.

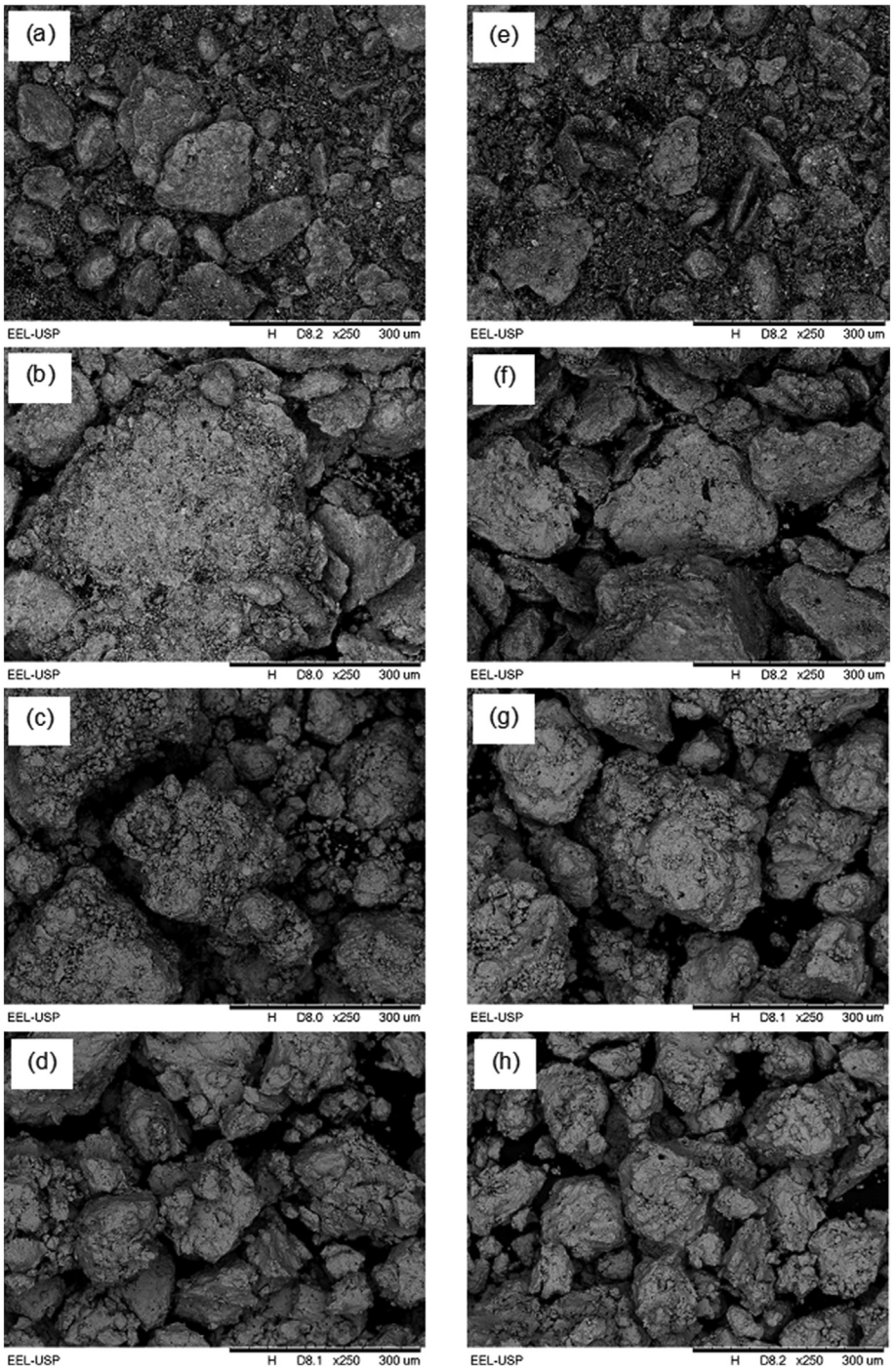

Fig. 4. SEM images of Ti-2Zn-22Si-11B and Ti-6Zn-22Si-11B powders at different milling times.

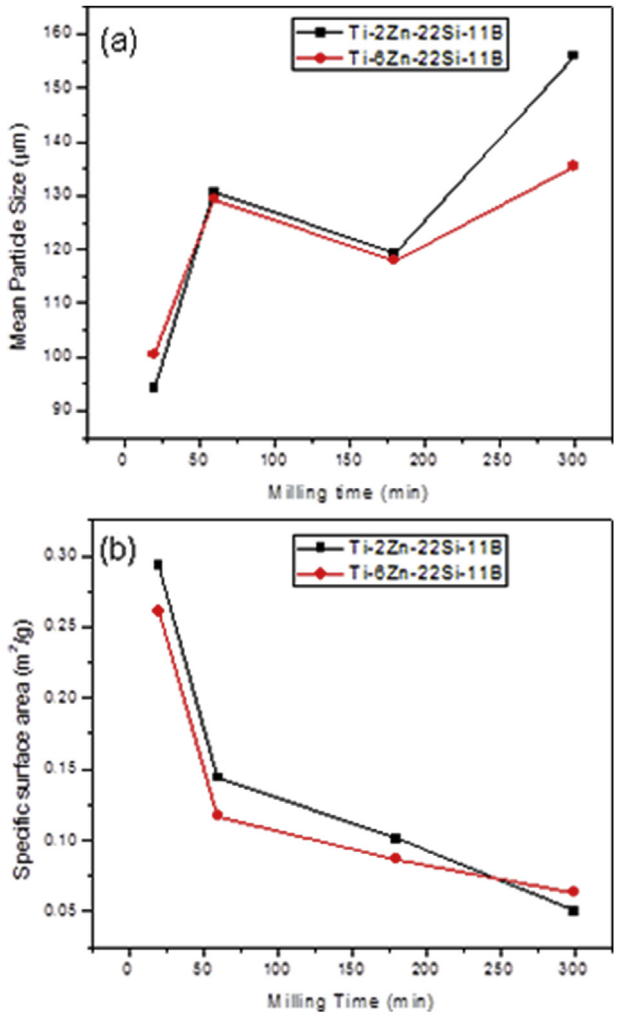

Fig. 5. Effect of composition and milling time on (a) particle size and (b) specific surface area of Ti-2Zn-22Si-11B and Ti-6Zn-22Si-11B powders at different milling times.

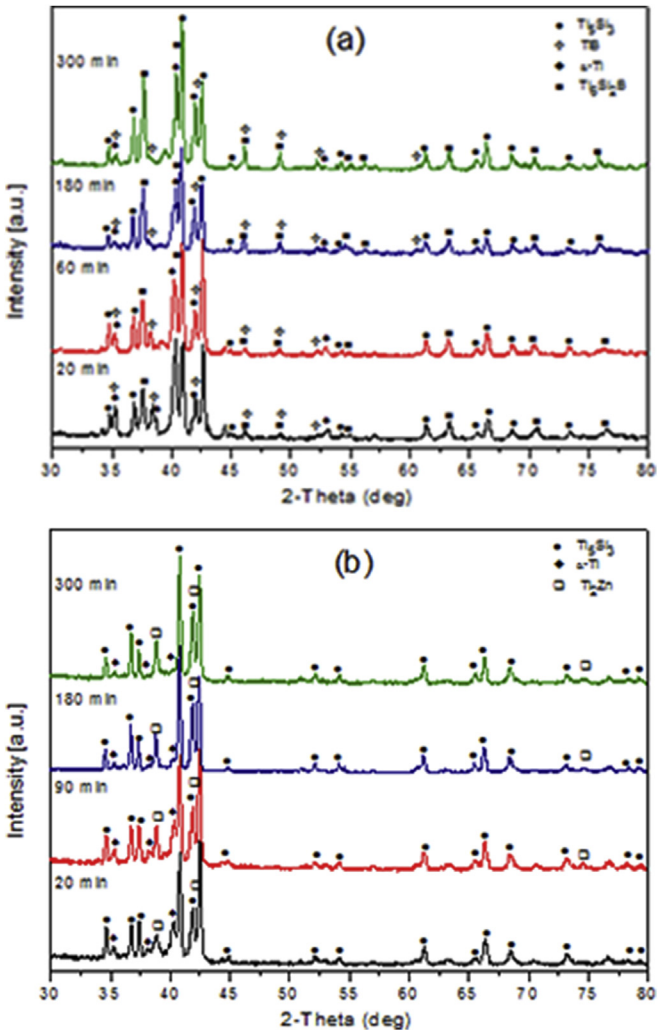

Fig. 6. XRD patterns of mechanically alloyed and spark plasma sintered Ti-2Zn-22Si-11B and Ti-6Zn-22Si-11B alloys.

SEM images of as-milled Ti-Zn-Si-B powders are illustrated in Fig. 4. Due to the large amount of ductile particles in starting powder mixtures, the particle sizes have increased during ball milling of the Ti-Zn-Si-B powder mixtures owing the occurrence of excessive cold welding mechanisms. Particles with flattened morphology was also observed in samples milled up to 60 min. After milling for 300 min, the particle sizes of rounded Ti-Zn-Si-B powders reduced, indicating that the equilibrium between the cold welding and fracture mechanisms was achieved. Fig. 5 shows the effect of composition and milling time on the particle size and specific surface area in Ti-2Zn-22Si-11B and Ti-6Zn-22Si-11B powders. According to the laser diffraction analysis, the average particle sizes (D50) of the Ti-2Zn-22Si-11B and Ti-6Zn-22Si-11B powder mixtures increased during milling from 94 (20 min) to 156 (300 min) micrometers and from 101 (20 min) to 136 (300 min) micrometers, respectively. Moreover, the powder particle sizes distributions were changed from bimodal to modal. Coherently, the average specific surface area of powder particles was continuously reduced during milling.

XRD patterns of spark plasma sintered Ti-2Zn-22Si-11B and Ti-6Zn-22Si-11B alloys previously milled at different times (20, 60, 180 and 300 min) are presented in Fig. 6a and b, respectively. Peaks of Ti, Ti_6Si_2B, TiB and Ti_5Si_3 were identified in the SPS Ti-2Zn-22Si-11B alloy while that the Ti_6Si_2B formation was inhibited in Zn-richer alloy. The Ti_2Zn peaks were also identified in XRD patterns of spark plasma sintered Ti-6Zn-22Si-11B alloy. The relative amount of crystalline phases in SPS samples is presented in Table 2. Owing to the short times adopted in SPS process, the amount of Ti_6Si_2B has increased in spark plasma sintered Ti-2Zn-22Si-11B samples with the increased milling time because its formation depends on occurrence of atomic diffusion mechanisms (Fig. 7a). It well known that more homogeneous materials can be reached at longer milling times as well as the diffusion path are also reduced in severely deformed microstructures. The TiB amounts smaller than 3% was measured in this quaternary alloy. In contrast, the spark plasma sintered Ti-6Zn-22Si-11B samples previously produced at longer milling times had increased the Ti_2Zn and Ti_5Si_3 amounts in detrimental to α-Ti (Fig. 7b).

Fig. 8 shows the SEM images of the spark plasma sintered Ti-2Zn-22Si-11B and Ti-6Zn-22Si-11B alloys and previously milled at different times (20, 60, 180 and 300 min). The Ti, Zn and Si contents measured by EDS analysis of phases formed in these alloys are

Table 2
Rietveld quantification of crystalline phases formed in the mechanically alloyed and spark plasma sintered Ti-2Zn-22Si-11B and Ti-6Zn-22Si-11B alloys.

	Milling time (min)	Ti_5Si_3; space group (193)	Ti - α; space group (194)	TiB; space group (62)	Ti_6Si_2B; space group (189)	Ti_2Zn; space group (139)	Rwp	Rexp	χ^2
65Ti-2Zn-22Si-11B	20	59.8%	21.9%	2.7%	15.6%	–	12.3	6.4	3.6
	60	49.7%	17.8%	2.4%	30.1%	–	12.4	7.1	3.0
	180	48.8%	17.2%	2.8%	31.2%	–	15.6	9.2	2.9
	300	53.0%	13.7%	3.6%	29.7%	–	12.1	7.0	3.0
62Ti-5Zn-22Si-11B	20	71.8%	24.4%			3.8%	14.5	9.3	2.4
	60	66.5%	22.7%			10.8%	16.9	8.7	3.8
	180	85.4%	2.3%			12.3%	17.8	7.1	4.4
	300	82.1%	2.0%			15.8%	17.4	9.6	3.3

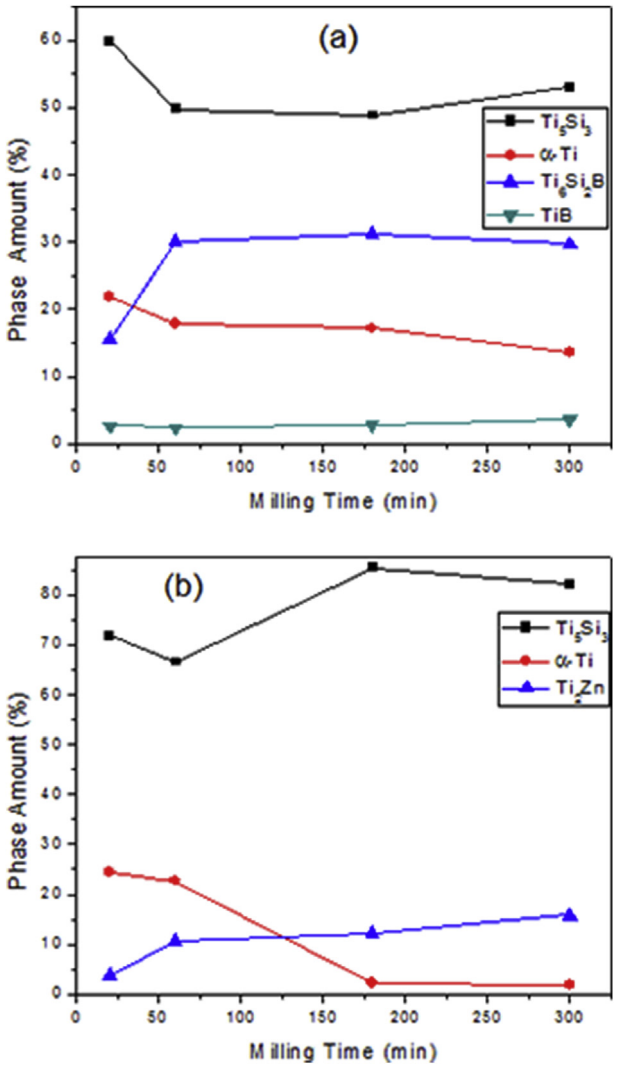

Fig. 7. Effect of composition and milling time on amount of crystalline phases in spark plasma sintered (a) Ti-2Zn-22Si-11B and (b) Ti-6Zn-22Si-11B alloys.

illustrated in Table 3. In SPS Ti-2Zn-22Si-11B alloy previously milled for 20 min, the Ti_{ss}, TiB, Ti_6Si_2B and Ti_5Si_3 phases have presented the Zn/Si contents of 3.1–4.3/2.6–3.8, 0.9–1.1/0.6–0.4, 1.0/27.1, and 1.5–1.2/36.1–32.7, respectively. $TiSi_2$ with 66.2 at.-% Si and 0.2 at.-% Zn was also detected in microstructure of this alloy owing to the short milling and SPS times providing features like in diffusion pairs from the elemental powder mixture. Such phases (except $TiSi_2$) dissolved higher Zn amounts in samples previously milled for 300 min: 4.2–8.5, 3.3–2.7, 1. 0–1.8, and 0.8–1.5, respectively. Similar results were found to α-Ti dissolving Zn contents close to 10 at.-% [25,26]. In spark plasma sintered Ti-6Zn-22Si-11B alloy, the Ti_6Si_2B phase was found in samples previously milled for 20 min only, which has dissolved 1.3 at;-% Zn. TiB and Ti_5Si_3 dissolved Zn contents between 0.5 and 3.9/1.1–3.6 and 2.5–3.2/3.2–4.8 in SPS Ti-6Zn-22Si-11B alloys previously milled for 20/300 min, respectively. EDS results of spark plasma sintering Ti-6Zn-22Si-11B samples previously milled for 20 and 300 min have also indicated the existence of Ti_3Zn in small regions dissolving up to 7 at.-% Si. Previous work has also suggested on its formation at low temperature [27].

Fig. 9 presents the Vickers hardness values of mechanically alloyed and spark plasma sintered Ti-2n-22Si-11B and Ti-6Zn-22Si-11B alloys. Excepting for the samples previously milled for 60 min, the spark plasma sintered Ti-2Zn-22Si-1B alloy presented mean values of Vickers hardness higher than 1050 HV, while that the mean values of Zn-richer samples were between 950 and 1050 HV. Results have indicated that the highest hardness were found in the Ti_6Si_2B-based alloys.

The high R_{wp} indices in the refinement obtained in this work are correlated with the contribution of the background, which wasn't removed from the raw data [3]. Nevertheless, the expected profile was close to that one weighted and the correlation between the R_{wp} and R_{exp} indices indicated a good fitness. For a matter of fact the χ^2 in most of the refined samples are smaller than 5 and that could be considered as quite good for common X-ray laboratory data.

4. Conclusions

Long times are required during ball milling of elemental Ti-Zn-Si-B powder mixtures in order to obtain the mechanical alloying needed during the short times adopted in spark plasma sintering.

Ti_6Si_2B dissolving between 1 and 1.8 at.% Zn was formed in microstructure of the Ti-2Zn-22Si-11B alloy only in which its amount was proportionally increased with the milling time.

In contrary, the Ti_5Si_3 and Ti_2Zn phases were preferentially formed in the spark plasma sintered Ti-6Zn-22Si-11B samples previously milled for 60–300 min, which dissolved zinc between 2.5 and 4.8 at.-%. Small Ti_3Zn amount was also identified in microstructures of these samples previously milled for 20 and 300 min.

The Ti-2Zn-22Si-11B alloy containing Ti_6Si_2B presented the Vickers hardness higher than 1050 HV while the Ti-6Zn-22Si-11B alloy between 950 and 1050 HV.

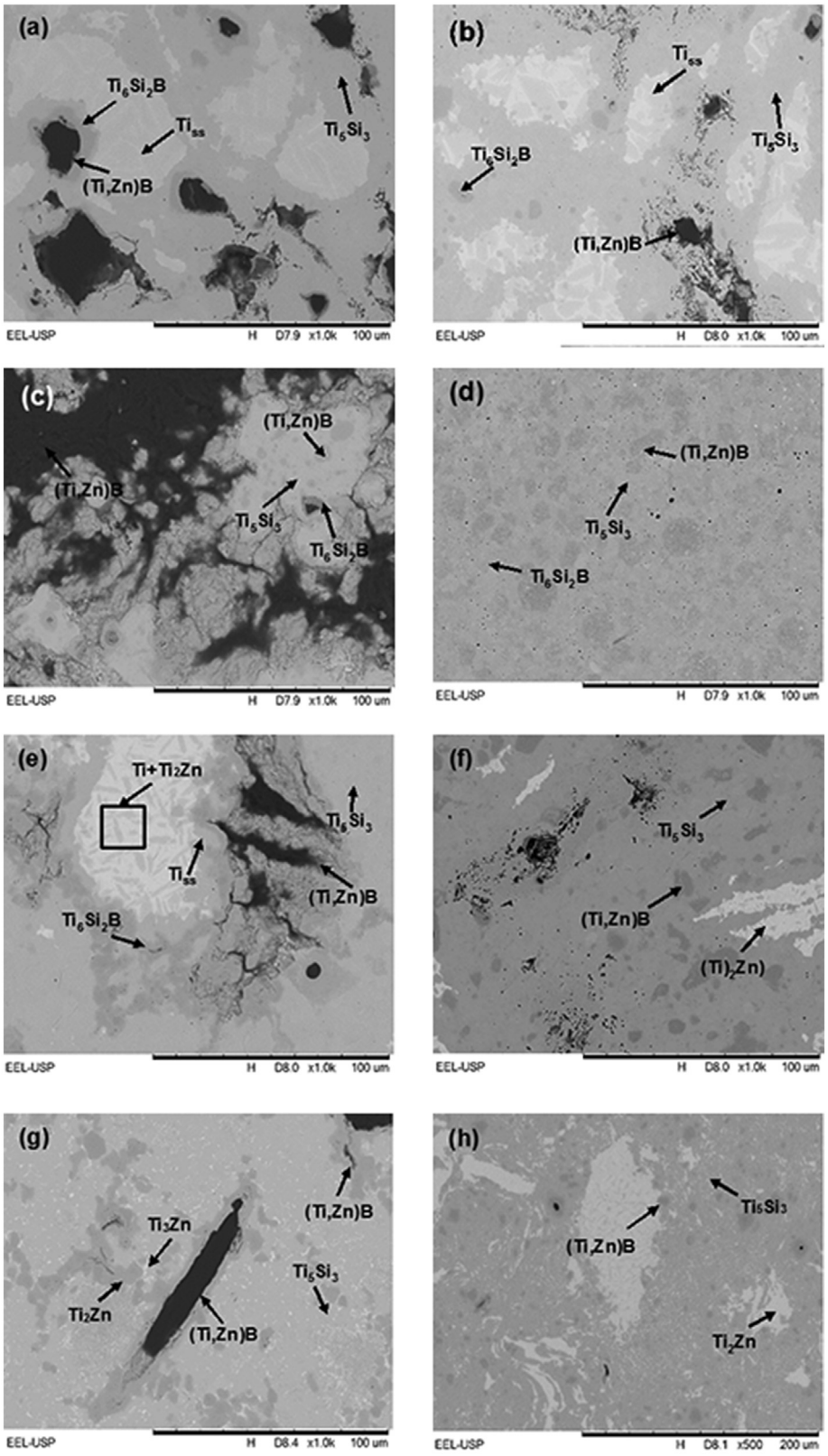

Fig. 8. SEM images of the mechanically alloyed and spark plasma sintered (a–d) Ti-2Zn-22Si-11B and (e–h) Ti-6Zn-22Si-11B alloys produced at different milling time: (a, e) 20 min, (b, f) 60 min, (c, g) 180 min, (d, h) 300 min.

Table 3
The Ti, Zn and Si contents measured by EDS analysis of phases formed in the mechanically alloyed and spark plasma sintered Ti-2Zn-22Si-11B and Ti-6Zn-22Si-11B alloys.

	Milling time (min)	Element	α-Ti (at.-%)	Ti_5Si_3 (at.-%)	Ti_6Si_2B (at.-%)	TiB (at.-%)	Ti_2Zn (at.-%)	Ti_3Zn (at.-%)
65Ti-2Zn-22Si-11B	20	Ti	94.3–91.9	62.4–66.1	71.9	98.2–98.0	–	–
		Zn	3.1–4.3	1.5–1.2	1.0	0.9–1.1	–	–
		Si	2.6–3.8	36.1–32.7	27.1	0.6–0.4	–	–
	180	Ti	–	60.5–62.7	73.1	95.2–99.2	–	–
		Zn	–	4.4–0.8	1.3	0.9–0.3	–	–
		Si	–	35.1–36.5	25.7	3.9–0.6	–	–
	300	Ti	94.5–88.6	63.3–62.3	72.1–73.9	95.2–95.8	–	–
		Zn	4.2–8.5	0.8–1.5	1.0–1.8	3.3–2.7	–	–
		Si	1.4–2.9	35.9–36.2	26.9–24.3	1.5	–	–
61Ti-6Zn-22Si-11B	20	Ti	88.0–95.3	64.8–65.1	76.2	98.6–94.8	–	81.5–78.8
		Zn	9.9–4.7	2.5–3.2	1.3	0.9–1.4	–	16.0–18.8
		Si	2.1–0	32.7–31.7	22.5	0.5–3.9	–	2.5–2.3
	180	Ti	–	62.1–62.9	–	98.3–97.8	73.1–66.1	–
		Zn	–	3.0–4.3	–	0.5–1.0	6.8–10.4	–
		Si	–	34.9–32.9	–	1.3–1.2	20.1–23.5	–
	300	Ti	–	62.9–61.2	–	97.1–95.1	66.1–69.4	73.8–73.5
		Zn	–	4.8–3.2	–	3.6–1.2	22.8–5.7	19.2–9.7
		Si	–	32.3–35.6	–	1.4–0.5	7.8–27.0	6.9–16.8

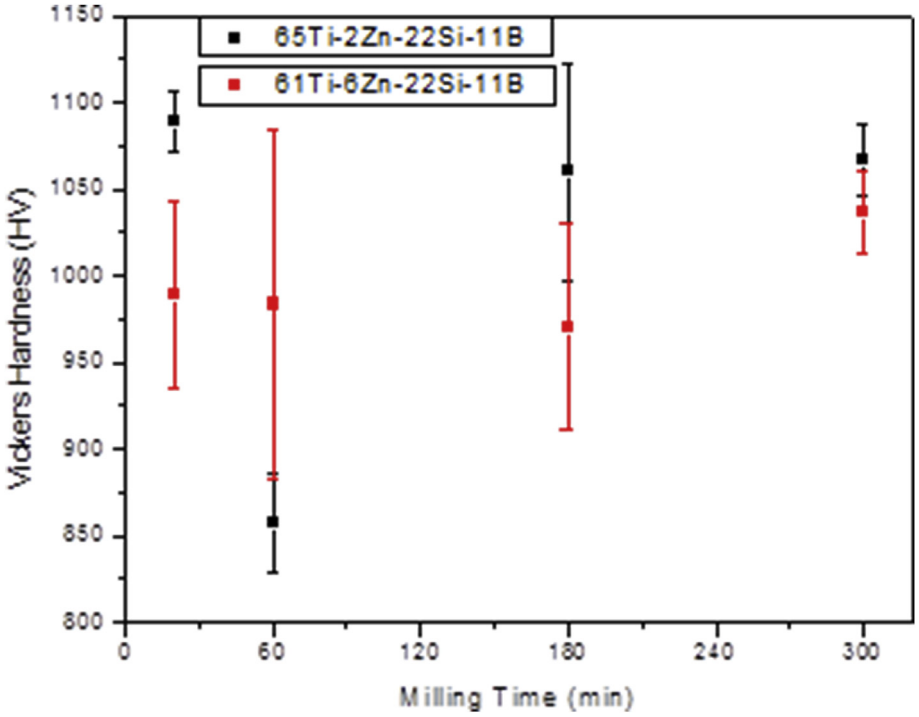

Fig. 9. Vickers hardness of mechanically alloyed and spark plasma sintered Ti-2n-22Si-11B and Ti-6Zn-22Si-11B alloys.

Acknowledgments

The authors thank the FAPESP-, FAPEMIG-, and CNPq-Brazil for financial supports used in this work.

References

[1] I. Kopova, J. Stráský, P. Harcuba, M. Landa, M. Janeček, L. Bačákova, Mat. Sci. Eng. C – Mater. 60 (2016) 230.
[2] M.T. Mohammed, Z.A. Khan, M. Geetha, A.N. Siddiquee, J. Alloys Compd. 634 (2015) 272.
[3] S. Ozan, J. Lin, Y. Li, Y. Zhang, K. Munir, H. Jiang, C. Wen, J. Mech. Behav. Biomed. 78 (2018) 224.
[4] M.T. Mohammed, Karbala Int. J. Modern Sci. 3 (2017) 224.
[5] Yu-yong Chen, Li-juan Xu, Zhi-guang Liu, Fan-tao Kong, Zi-yong T. Chen, Nonferrous Metal. Soc. 16 (2006) s824.
[6] L. Kunčická, R. Kocich, T.C. Lowe, Prog. Mater. Sci. 88 (2017) 232.
[7] A.S. Ramos, C.A. Nunes, G. Rodrigues, P.A. Suzuki, P. Rogl, Intermetallics 12 (2004) 487.
[8] A.N. Silva, G. Silva, A.S. Ramos, A.L. Paschoal, E.C.T. Ramos, M. Filgueira, Intermetallics 14 (2006) 585.
[9] M.K.N. Kato, E. Onari, E.A.L. Arisawa, N.S. Silva, A.S. Ramos, Mat. Sci. Eng. C – Mater. 29 (2009) 980.
[10] B.B. Fernandes, R.M. Oliveira, M. Ueda, S.F.M. Mariano, A.S. Ramos, M.S. Vieira, F.C.L. Melo, G. Oliveira, Surf. Coating. Technol. 228 (2013) 195.
[11] A.S. Ramos, C.A. Nunes, G. Rodrigues, E.C.T. Ramos, J. Alloys Compd. 601 (2014) 94.
[12] A.C. Zanardo, N.A. Mariano, L.B. Alkmin, A.M.S. Costa, C.A. Nunes, A.S. Ramos, Mater. Sci. Forum 802 (2014) 9.
[13] L.M. Ferreira, L.B. Alkmin, E.C.T. Ramos, C.A. Nunes, A.S. Ramos, Mater. Sci. Forum 802 (2014) 20.
[14] D.K. Khajuria, C. Disha, R. Vasireddi, R. Razdan, D.R. Mahapatra, Mat. Sci. Eng. C – Mater. 63 (2016) 78.
[15] G.P. Vassilev, X.J. Liu, K.J. Ishida, Alloys Compd. 375 (2004) 162.
[16] H. Okamoto, Binary Alloy Phase Diagr. 1 (1990) 559.
[17] R.W. Olesinski, G.J. Abbaschian, Bull. Alloy Diagr. 6 (1985) 545.
[18] H.M. Rietveld, A profile refinement method for nuclear and magnetic structures, J. Appl. Crystallogr. 2 (1969) 65–71.

[19] R.J. Hill, C.J. Howard, Quantitative phase Analysis from neutron powder diffraction data using the rietveid method theory, J. Appl. Crystallogr. 20 (1987) 467–474.
[20] U. Holzworth, N. Gibson, The Scherrer equation versus the 'Debye-Scherrer equation', Nat. Nanotechnol. 6 (2011) 534.
[21] B.H. Toby, R factors in Rietveld analysis: how good is good enough? Powder Diffr. 21 (2006) 67–70, https://doi.org/10.1154/1.2179804.
[22] L.B. Mccusker, R.B. Von Dreele, D.E. Cox, D. Loue, P. Scardi, Rietveld refinement guidelines, Int. Union Crystallogr. J. Appl. Crystallogr. J. Appl. Cryst. 32 (1999) 36–50, https://doi.org/10.1107/S0021889898009856.
[23] H.M. Rietveld, A profile refinement method for nuclear and magnetic structures, J. Appl. Crystallogr. 2 (1969) 65–71, https://doi.org/10.1107/S0021889869006558.
[24] ASTM: C-1327-15, Standard Test Method for Vickers Indentation Hardness of Advanced Ceramics, 2015, pp. 1–8.
[25] G. Ghosh, S. Delsante, G. Borzone, M. Asta, R. Ferro, Phase stability and cohesive properties of Ti–Zn intermetallics: first-principles calculations and experimental results, Acta Mater. 54 (2006) 4977–4997.
[26] D.A. Brice, P. Samimi, I. Ghamarian, Y. Liu, M.Y. Mendoza, M.J. Kenney, R.F. Reidy, M. Garcia-Avila, P.C. Collins, On the eutectoid transformation behavior of the Ti-Zn system and its metastable phases, J. Alloys Compd. (2017), https://doi.org/10.1016/j.jallcom.2017.05.103.phases.
[27] Roman V. Chepulskii, Stefano Curtarolo, Calculation of Solubility in Titanium Alloys from First-Principles, 1 Jan 2009 arXiv:0901.0200v1 [cond-mat.mtrl-sci].